ADVANCED MATERIALS INTERFACES
Open Access
www.advmatinterfaces.de

Poly(Amino Acid) LbL Multilayers With Embedded Silver and Copper Oxide Nanoparticles as Biocompatible Antibacterial Coatings

*Ana-Marija Milisav, Lamborghini Sotelo, Cristina Cantallops-Vilà, Tommaso Fontanot, Ina Erceg, Krunoslav Bojanić, Tomislav Vuletić, Željka Fiket, Maja Ivanić, Silke Christiansen, Edwige Meurice, and Maja Dutour Sikirić**

The growing concern over implant-associated infections motivates the development of novel antibacterial coatings for medical devices as an effective strategy in reducing the occurrence of IAI. Polyelectrolyte multilayers (PEMs) incorporating metal/metal oxide nanoparticles (NPs) as antimicrobial components receive special attention for their ability to coat diverse surface types and low potential to induce antimicrobial resistance. This study investigates the potential of poly(amino acid) multilayers consisting of poly-L-lysine and poly-L-glutamic acid with embedded silver (PEMAg) or copper oxide (PEMCuO) deposited on titanium surfaces for the coating of medical surfaces. The results of the quartz crystal microbalance with dissipation, scanning electron microscopy, and electron dispersive spectroscopy show that both types of NPs are successfully incorporated in the PEM and deposited over the entire coated surface. The incorporation of NPs in PEM prevents the burst release. The viability of MG-63 cells is higher than 70% on all investigated PEMs, confirming their biocompatibility. PEMCuO shows better biofilm prevention compared to PEMAg, entirely preventing *Pseudomonas aeruginosa* biofilm and allowing the formation of only weak *Staphylococcus aureus* biofilm. The results obtained confirm the high potential of poly(amino acids) multilayers with embedded metal/metal oxide NPs as biocompatible antimicrobial coatings for medical devices.

1. Introduction

In modern medical practice, the use of implantable medical devices has become a common procedure to maintain a patient's physiological functions after a serious illness or injury.[1] These devices notably improve the quality of life of patients over the age of 50 who are affected by chronic conditions.[2,3] However, implant-associated infections (IAIs) are considered a major drawback of implantation, which can endanger the patient, prolong medical treatment, and significantly increase its cost.

The adhesion of pathogenic bacteria to the surface of the medical device is the first step that can lead to IAIs. Once adhered, bacteria can proliferate and form biofilms.[4] These biofilms hinder the penetration of antimicrobial agents and induce their metabolic transformation, reducing the efficacy of treatments and leading to persistent, difficult-to-treat infections. As a result,

A.-M. Milisav, I. Erceg, K. Bojanić, Ž. Fiket, M. Ivanić, M. Dutour Sikirić
Ruđer Bošković Institute
Bijenička cesta 54, Zagreb 10000, Croatia
E-mail: sikiric@irb.hr
L. Sotelo
Friedrich-Alexander-Universität Erlangen-Nürnberg
Staudtstraße 7, 91058 Erlangen, Germany
L. Sotelo, S. Christiansen
Innovations-Institut für Nanotechnologie und Korrelative Mikroskopie eV
INAM
Äußere Nürnberger Str. 62, 91301 Forchheim, Germany
C. Cantallops-Vilà, E. Meurice
Université Polytechnique Hauts-de-France
6 rue de Rambouillet, Cambrai 59400, France
T. Fontanot, I. Erceg, S. Christiansen
Fraunhofer Institute for Ceramic Technologies and Systems IKTS
Äußere Nürnberger Str. 62, 91301 Forchheim, Germany
T. Vuletić
Institute of Physics
Bijenička cesta 46, Zagreb 10000, Croatia

The ORCID identification number(s) for the author(s) of this article can be found under https://doi.org/10.1002/admi.202400631

DOI: 10.1002/admi.202400631

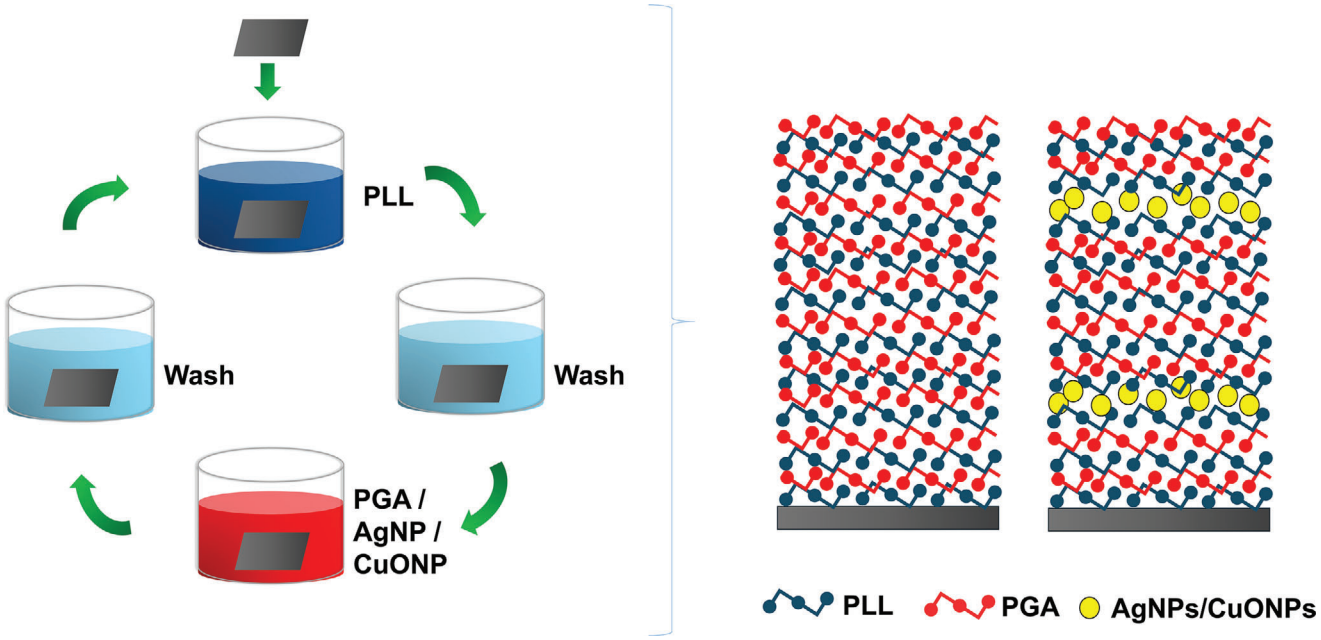

Figure 1. Scheme depicting the layer-by-layer build-up of poly-L-lysine (PLL) and poly-L-glutamic acid (PGA) multilayers with and without embedded silver (AgNPs) and copper oxide (CuONPs) nanoparticles. The process begins with depositing PLL (blue) by immersing the substrate in a PLL solution, followed by washing with a buffer to remove excess material. Next, PGA (red) is deposited, and the substrate is washed again. This process is repeated, with AgNPs and CuONPs embedded during the deposition of the 3rd and 8th bilayers by immersing the substrate into either AgNPs or CuONPs suspension. The right-hand side of the figure shows the final multilayer structures: one with 10 PLL/PGA bilayers without nanoparticles and another with either silver or copper oxide nanoparticles incorporated.

much higher doses of antibiotics are required to treat bacterial biofilms than to treat the same bacteria in their planktonic form.[5] It is estimated that biofilm formation is responsible for 80% of all hospital-acquired microbial infections, which can lead to chronic infections and severe tissue damage.[1,4]

Traditional treatments for IAIs often involve prolonged systemic administration of antibiotics.[6] However, decades of overuse of antibiotics have led to the development of bacterial resistance, so the number of infections caused by antibiotic-resistant bacteria is constantly increasing, posing a major challenge for both patients and healthcare systems.[7,8] Consequently, the functionalization of medical device surfaces with antimicrobial agents has become a major research focus, aiming to prevent adverse outcomes and provide a more sustainable solution.[1,9–11]

Among the various materials, metal/metal oxide nanoparticles are attracting attention because of their antimicrobial efficacy and the lower likelihood of bacterial resistance due to their multiple simultaneous mechanisms of action.[12] Silver and copper/copper oxide nanoparticles are among the most commonly used nanoparticles for the preparation of materials with antimicrobial properties. The broad-spectrum antimicrobial activity of silver has long been recognized.[13–15] The advantage of silver nanoparticles (AgNPs) is the release of Ag^+ ions, making them more active than bulk silver.[16] Although AgNPs are unlikely to induce bacterial resistance,[17] there is evidence to the contrary.[18] This finding has motivated research on other types of metal/metal oxide nanoparticles. Copper is another material whose antimicrobial activity was recognized early in human history.[19] The copper/copper oxide nanoparticles (CuNPs/CuONPs) are receiving attention because copper is crucial for many cellular enzymes and major physiological functions, such as angiogenesis, immune response, bone mineralization, and osteoblast function.[20–22] Furthermore, dietary excess[23] or skin contact[24] are unlikely to harm mammals. Like silver, copper has broad-spectrum antimicrobial activity, and some studies claim it is more efficient than silver.[19] Additionally, CuNPs release ions at a much faster rate than AgNPs.[25,26]

Consequently, various techniques have been developed to introduce of silver and copper nanostructures to the surfaces of medical implants.[27] However, due to the potential cytotoxicity of nanoparticles released into the system/organism, studies suggest that nanoparticles should be embedded in a matrix to reduce adverse effects and ensure biocompatibility.[28]

Among different matrices, polyelectrolyte multilayers (PEMs) attract special attention and are commonly used for the preparation of antimicrobial coatings.[29] Their build-up on the substrate is performed by the sequential adsorption of oppositely charged polyelectrolytes, known as the layer-by-layer (LbL) method.[30] This LbL method is versatile, as it can be applied to almost any type of substrate, regardless of its size, shape, topology or composition. The properties of PEMs (chemical, physicochemical, and mechanical) can be tailored by varying their building components and preparation conditions (solvent, pH, temperature, ionic strength).[31] In addition, active components (different chemical compounds, bioactive macromolecules, nanoparticles, etc.) can be incorporated into PEMs and their release can be sustained. Thus, special attention is given to PEMs containing inorganic nanomaterials, as such hybrid coatings have specific properties of interest for the development of new photonic materials, sensors and biosensors, transistors, amplifiers, and

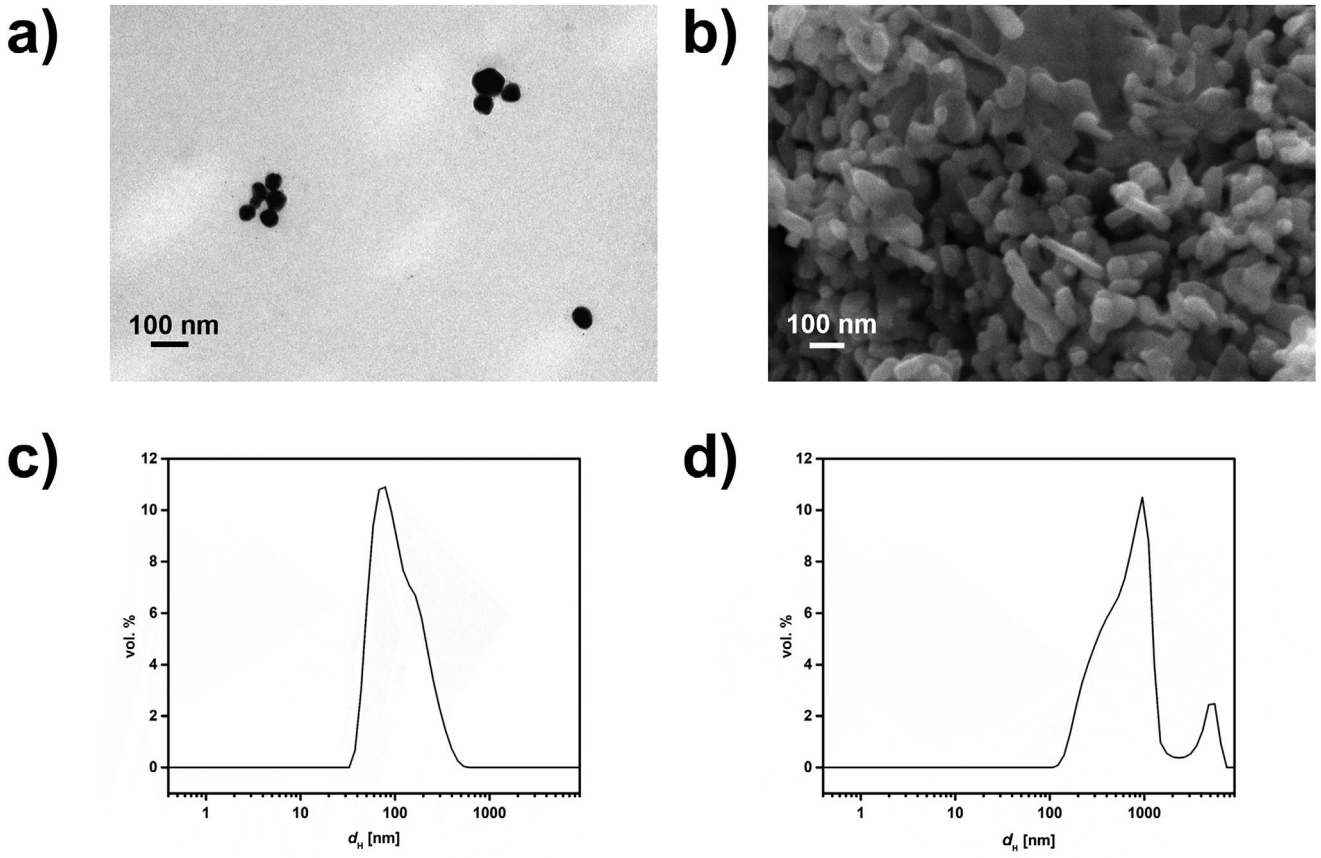

Figure 2. a) TEM micrograph of polyvinylpyrrolidone (PVP) stabilized silver nanoparticles (AgNPs), b) SEM micrograph of copper oxide nanoparticles (CuONPs), and representative volume size distribution of c) AgNPs and d) CuONPs suspended in HEPES/NaCl buffer at 25 °C, pH 7.4, γ(AgNPs) = γ(CuONPs) = 50 mg dm^{-3}, d_h – hydrodynamic diameter.

biomaterials.[32,33] The application field can be further expanded by combining the LbL method with techniques like spin-coating, photolithography, and spraying.[34]Therefore, it is not surprising that the application of PEMs in the coating of various medical devices, including bone implants, catheter tubes, intraocular lenses, and suture membranes, is the subject of numerous research.[29,35]

Previous studies have investigated AgNPs synthesized in situ within PEMs, mainly by the reduction of Ag^+ ions,[36–43] and less frequently by incorporation as the anionic component of the multilayer, based on the negative charge of the nanoparticles.[44] To the best of our knowledge, only a few studies have examined the incorporation of copper nanoparticles into PEMs.[45,46] Although these studies were aimed at producing antimicrobial coatings, only a few of them evaluated biocompatibility, a fundamental property of implantable medical devices.[38,41,46,47] Furthermore, even though the type of substrate may substantially influence PEM properties,[48] only two studies[39,46] used common implant materials as substrates. To the best of our knowledge, no study has investigated poly(amino acids) as matrices for the incorporation of nanoparticles, despite their significant advantage for biomedical applications due to their biocompatibility and biodegradability, as they metabolize naturally within biological systems, reducing the risk of long-term toxicity.[49] Poly(amino acids) secondary structures are similar to structural motifs in natural proteins, allowing them to mimic biological processes and making them valuable for creating biomimetic materials that interact effectively with biological tissues.[31]

Motivated by this lack of data, this study aims to investigate the potential of poly(amino acid) multilayers as matrices for the incorporation of AgNPs or CuONPs and to determine the physicochemical properties and biological performance of these two types of coatings. Poly-L-lysine (PLL) and poly-L-glutamic acid (PGA) were chosen for the build-up of the PEMs because they are known to form biocompatible PEMs.[50] In addition, the PEMs ending in negatively charged PGA were chosen to utilize the repulsive forces between negatively charged PEM and bacterial cell membranes to further enhance antibacterial activity.[46,51] Synthesized AgNPs stabilized with polyvinylpyrrolidone (PVP) and commercial CuONPs were embedded as anionic components of the PEMs to avoid in situ synthesis and possible traces of reducing agents. Due to the differences between the nanoparticles, only their individual contributions to the properties of the multilayers were investigated in the current study. **Figure 1** depicts the build-up process and multilayer composition. As titanium is a widely used material for medical implants due to its excellent biocompatibility and mechanical properties,[52] it was chosen as the substrate in this study unless limited by the specificity of the

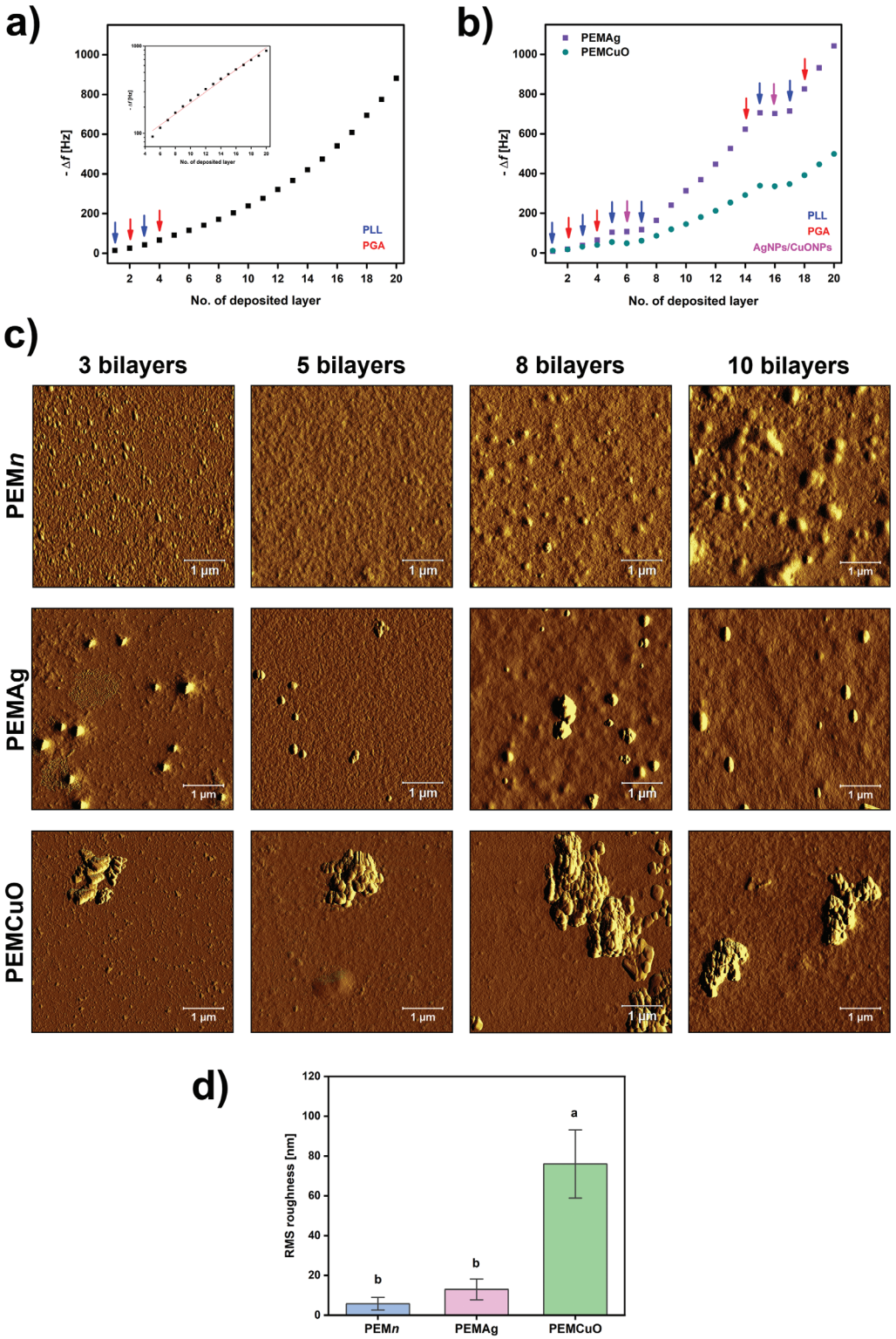

Figure 3. Changes in frequency shift ($-\Delta f$) and surface characteristics of poly-L-lysine (PLL) and poly-L-glutamic acid (PGA) multilayers. Increase in $-\Delta f$ with the number of deposited PLL and PGA layers a) without nanoparticles (PEM*n*), including an inset log/lin graph confirming the exponential growth due to swelling, b) with silver (PEMAg) and copper oxide nanoparticles (PEMCuO). c) AFM amplitude images of the 3, 5, 8, and 10 deposited PLL/PGA bilayers without (PEM*n*) and with nanoparticles (PEMAg and PEMCuO). d) RMS roughness analysis of PEM*n*, PEMAg, and PEMCuO. Arrows denote the addition of PLL (blue), PGA (red), AgNPs, and CuONPs (magenta). Error bars represent standard error. Means with different letters are significantly different, $p \leq 0.05$. γ (PLL) = (PGA) = 1 mg mL^{-1}, γ (AgNPs) = (CuONPs) = 50 mg L^{-1}, HEPES/NaCl buffer, pH 7.4, 23 ± 0.02 °C.

research method. The viability of osteoblast MG-63 cells was assessed to determine the biocompatibility of prepared coatings. Two common pathogens in IAIs,[53] namely *Staphylococcus aureus* and *Pseudomonas aeruginosa*, were used in biofilm formation assay.

2. Results

2.1. Characterization of AgNPs and CuONPs

Two types of nanoparticles, AgNPs and CuONPs, known for their antibacterial properties were used for PEMs build-up. The morphology and primary size of the AgNPs were determined by transmission electron microscopy (TEM) while scanning electron microscopy (SEM) was used for CuONPs, as it was shown to be the more appropriate method (**Figure** 2a,b). The AgNPs were found to be predominantly polyhedral particles with an average size of 54.7 ± 9.5 nm. In the case of CuONPs, a mixture of rod-shaped and irregular plate-shaped particles with an average size of 114.2 ± 17.9 nm in size was observed.

Considering that nanoparticles tend to agglomerate in media with high ionic strength due to the screening of electrostatic interactions,[54,55] the behavior of AgNPs and CuONPs in HEPES/NaCl buffer (media for multilayer build-up) was investigated using dynamic light scattering (DLS) and electrophoretic light scattering (ELS). In the AgNPs suspension, a dominant population of particles with d_h 121.7 ± 3.0 nm, indicating the quality of synthesis and stability, was detected (Figure 2c). A population of larger particles with d_h ≈5000 nm was also detected, but in low amounts (1.8 vol. %). The zeta potential of the AgNPs was −8.0 ± 0.8 mV.

In contrast to the AgNPs, the CuONPs aggregated in HEPES/NaCl buffer (Figure 2d). A bimodal size distribution was observed, with a dominant population of particles with a hydrodynamic diameter of 676.0 ± 60.0 nm and a population of particles with an average hydrodynamic diameter of 4958.8 ± 434.1 nm present in 7.4 ± 2.1 vol. %. The zeta potential of the CuONPs was −15.5 ± 2.6 mV.

2.2. PEMs Build-Up and Physico-Chemical Properties

Figure 1 shows the in situ build-up of PLL/PGA PEMs: without nanoparticles (PEM*n*), with embedded AgNPs (PEMAg) and CuONPs (PEMCuO), monitored using quartz-crystal microbalance with dissipation monitoring (QCM-D). During the measurement of the PLL/PGA multilayer build-up, each PLL or PGA adsorption step was marked by a decrease in oscillating resonance frequency (Δf), indicating mass changes, and an increase in dissipation (ΔD), reflecting viscous losses within the multilayer shown in Figure S1a (Supporting Information). A slight increase in Δf accompanied by a decrease in ΔD was noted during the buffer rinsing steps, suggesting slight desorption of loosely attached polyelectrolyte molecules and the establishment of a more compact multilayer, consistent with previous reports.[56] Overall, the PLL/PGA multilayer showed an exponential growth regime (**Figure** 3a), which is consistent with previous observations.[57–59] This suggested that the final layers contribute much more to the mass and dissipation changes than the initial ones, indicating that the final layers are more hydrated and swollen.[31] The final thickness of the hydrated PLL/PGA multilayer was calculated to be 153.77 ± 5.08 nm using the Voigt model, as the dissipation changed distinctly ($\Delta D > 0$).[60] Previous studies have shown that the thickness of PEM depends on the experimental conditions (pH and ionic strength, molecular weight of the polyelectrolyte, and the type and concentration of salts used) as well as on the measurement method.[31,61] Lavalle et al. reported a thickness of ≈300 nm for $(PLL/PGA)_8$ multilayers measured by optical waveguide light-mode spectroscopy, but only 160 nm was measured for 10 bilayers by AFM.[57] On the other hand, Richert et al.[58] showed that polyethylenimine (PEI)-$(PLL/PGA)_{10}$ multilayers built in water at a pH of 7.4 are extremely thin, reaching a thickness of ≈15 nm, while Halthur and Elofsson[62] reported a thickness of 30 nm for PEI-$(PLL/PGA)_6$ PEM prepared in buffer at a pH of 7.4.

Since both types of nanoparticles exhibited a negative zeta potential in HEPES/NaCl buffer, the medium used for the PEM build-up, their suspensions were used as anionic components instead of the PGA solution during the 3rd and 8th bilayer build-up. The corresponding frequency and dissipation changes observed in PLL/PGA multilayers with nanoparticles are shown in Figure 3b and Figure S1b,c (Supporting Information). It is noteworthy that the changes in Δf after adsorption of AgNPs and CuONPs were negligible. This indicates that the nanoparticle coverage was probably a submonolayer with a relatively small amount of adsorbed material.

The dissipation energy parameter (ΔD) revealed more details about the adsorption behavior of nanoparticles. As shown in Figure S1b,c (Supporting Information), the deposition of nanoparticles in the 3rd PLL/PGA bilayer notably contributed to the overall viscoelastic response. Effectively, they adsorbed on the top of the multilayer and remain in a state of minimal binding, reducing the oscillations of the quartz crystal. In contrast, when the nanoparticles were deposited in the 8th bilayer, they did not contribute to the dissipation parameter of the multilayer, i.e., ΔD is negligible. Since the higher layers are swollen and the polyelectrolyte chains are uncoiled, the entire structure is more open.[31,56–59] It can be assumed that the nanoparticles were embedded within this open multilayer structure, concealed and thereby not influencing dissipation.[63] This type of bonding limits thickness modeling by QCM-D.

The development of topography of the PEMs was visualized by atomic force microscopy (AFM, Figure 3c), imaging PEMs after the deposition of the 3rd, 5th, 8th, and 10th bilayer. For the PEM*n* samples, AFM images revealed that with the increasing layers, the PLL/PGA multilayer became increasingly granular, with both the width and height of the granules expanding, as previously observed.[57] In the case of PEMAg, after the first adsorption of AgNPs (3rd bilayer), AgNPs were visible as sparsely distributed individual nanoparticles on the surface, confirming the QCM-D results. The granular morphology of the PEM was observed between AgNPs and became more pronounced after the deposition of the 5th bilayer. The subsequent deposition of AgNPs (8th bilayer) resulted in a notably larger height of the nanoparticles and their aggregation, while the PEM remained visible, especially after the deposition of the 10th bilayer.

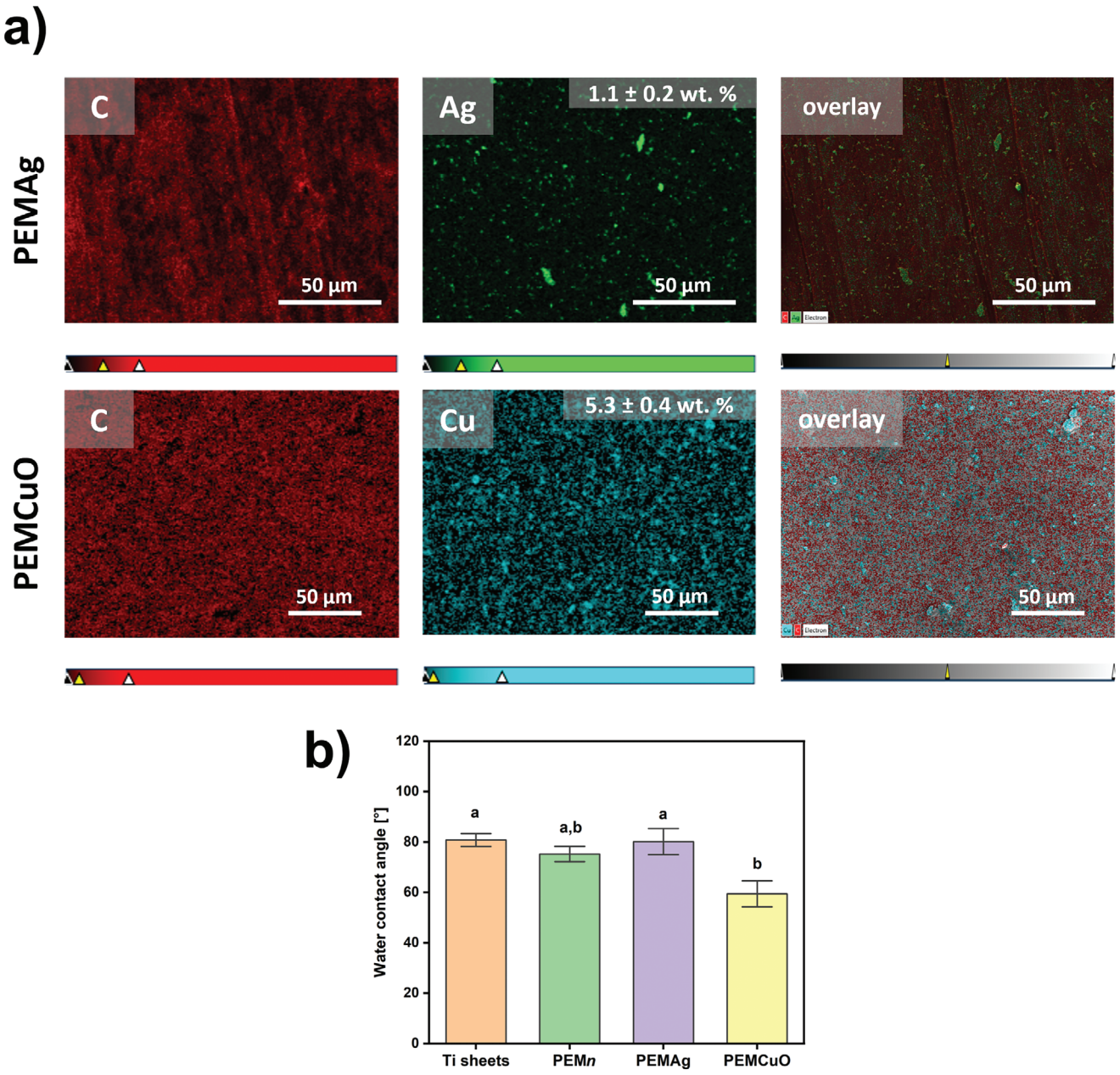

Figure 4. a) Energy dispersive X-ray spectroscopy elemental maps of carbon (red), silver (green), and copper (blue) obtained from poly-L-lysine (PLL) and poly-L-glutamic acid (PGA) multilayers consisting of 10 bilayers with incorporated silver (PEMAg) and copper oxide nanoparticles (PEMCuO) deposited on titanium substrates. Each map is displayed in the relative intensity scale where the color of each element is presented in strong, bright (element-rich), and dark (element-deficient) colors. c) Water contact angle of Ti sheets, PLL/PGA multilayers consisting of 10 bilayers without nanoparticles (PEM*n*), and with nanoparticles (PEMAg, PEMCuO). Error bars represent standard error. Means with different letters are significantly different, $p \leq 0.05$.

Concerning CuONPs adsorption, CuONPs aggregates were readily adsorbed in the first deposition step (3rd bilayer), growing larger after the second deposition step (8th bilayer). The AFM images of PEMCuO show the formation of larger aggregates than PEMAg, which can be attributed to the inherent differences in the nanoparticles themselves. As can be seen in Figure 2a,b, the nanoparticles differ substantially in shape and size, with the AgNPs exhibiting a relatively monodisperse distribution. In contrast, a pronounced polydispersity in size and shape was observed for the CuONPs. These differences between the nanoparticles were reflected in their surface adsorption behavior and contributed to the observed differences in the coating topographies. Previous studies have shown that the size of the nanoparticles affects the density and thickness of the films as well as the adsorption kinetics. In the presence of smaller particles, smoother, denser films with more nanoparticles were obtained.[64] It should be noted that in biomedical applications, the reduction in nanoparticle size may be limited by the increasing

Table 1. Amount of silver and copper incorporated in poly-L-lysine and poly-L-glutamic acid multilayers consisting of 10 bilayers with incorporated silver (PEMAg) or copper oxide nanoparticles (PEMCuO), and the cumulative amount of silver and copper released from the respective coating during 24 h exposure to phosphate buffer saline at 37 °C.

Sample	Incorporated [μg cm^{-2}]	1 h release [μg cm^{-2}]	4 h release [μg cm^{-2}]	24 h release [μg cm^{-2}]
		Ag		
PEMAg	2.585 ± 0.529	0.052 ± 0.003	0.115 ± 0.009	0.233 ± 0.043
		Cu		
PEMCuO	7.323 ± 0.760	0.020 ± 0.004	0.092 ± 0.048	0.150 ± 0.033

toxicity with decreasing size.[25] It was proposed that embedding into polymer matrices, in general, could be a way of reducing nanoparticle cytotoxicity.[28] A similar agglomeration of CuONPs was previously observed in poly(allylamine hydrochloride) (PAH)/alginate multilayer.[46]

The observed differences in the topography of PEMs were reflected in Root Mean Square (RMS) values (Figure 3d). The lowest RMS values were observed for the PEM*n*, indicating a relatively smooth surface texture. Although the RMS value for PEMAg was higher than for PEM*n* coatings, the difference was not significant. However, PEMCuO exhibited the highest RMS roughness value, indicating a significantly rougher surface texture. The high roughness and standard deviation obtained for this coating indicate variability in the surface properties of the sample, probably due to the pronounced surface irregularities caused by adsorbed CuONPs aggregates.

To confirm the incorporation of AgNPs and CuONPs within the PEM, energy dispersive spectroscopy (EDS) was performed. The spatial distribution of carbon (C), silver (Ag), and copper (Cu) is shown in **Figure** 4a. The mapping of C in both cases confirmed the formation of the PEMs over the entire substrate surface. In the presence of CuONPs, the PEM appeared denser and more homogeneous. Ag mapping revealed that both AgNPs and their aggregates were distributed throughout the PEM. The CuONPs appeared to be more aggregated and more densely adsorbed. The larger adsorption of CuONPs compared to AgNPs was confirmed by the average weight %, that is, 1.1 wt. % of Ag and 5.3 wt. % of Cu was embedded within the corresponding PEM.

To determine the amount of AgNPs and CuONPs incorporated within the coatings, the coatings were dissolved in nitric acid. To ensure accuracy, bare Ti sheets underwent the same dissolution procedure, and the resulting values were used as baseline correction for the measurements of the coated surfaces. The inductively coupled plasma mass spectrometry (ICP-MS) results confirmed that the PEM coatings incorporated a higher amount of CuONPs compared to AgNPs (**Table 1**). These findings align with those of Kruk et al.[44] who reported that the amount of Ag in PEI/AgNPs PEM ranged from 500 ng cm^{-2} to 15100 ng cm^{-2}, which is comparable to our results.

Around 10% of the incorporated Ag and only 2% of Cu ions were released within 24 h, with both types of PEMs showing rapid release within the initial 4 h, followed by gradual release up to 24 h. Considering the low release amounts, it is noteworthy that burst release is prevented and that these coatings enable slow release over time, which is important for the development of controlled release systems. This release behavior is in contrast to the findings of Wang et al.[38] who observed burst release from chitosan-Ag/PVP nanocomposite films within the first day. However, they also observed that Ag^+ ions exceeded the minimum inhibitory concentration of Ag^+ (0.12 mg L^{-1}) over the following 26 days. It is important to note that only the total release of Ag and Cu was determined in our study, as the samples were dissolved in nitric acid and thus it was not possible to detect the release of nanoparticles themselves.

Water contact angle measurements revealed the influence of different surfaces on wettability (Figure 4b). Coating Ti sheets with PEM*n* slightly reduced the water contact angle from 80.8 ° ± 5.4 ° to 75.2 ° ± 5.8 °. The incorporation of AgNPs and CuONPs into the PEMs resulted in different effects. PEMAg demonstrated a slight increase in contact angle to 80.1 ° ± 9.7 ° compared to PEM*n*. A similar trend of water contact angle change upon incorporation of AgNPs was previously observed with dopamine-modified alginate/chitosan PEM.[39] However, incorporating CuONPs into PEM resulted in a statistically significant reduction in water contact angle to 59.4 ° ± 11.4 °, indicating improved wettability of the PEMCuO-coated surfaces. Previously, it had been suggested that an increase in water contact angle could be a consequence of changes in the polyelectrolyte orientation within the PEM, leading to greater exposure of the polymer backbone than the functional groups on the surface of the film. Contrary, the presence of metal ions or nanoparticles near the surface could lead to a decrease in the water contact angle.[37] The improved wettability could also be related to the higher surface roughness[65] of PEMCuO.

2.3. Biocompatibility Assessment

As already mentioned, biocompatibility is a key requirement for medical devices that are to be implanted in the human body. To assess the biocompatibility of the developed material, the viability of osteoblastic MG-63 cells of uncoated and PEM*n*-, PEMAg- and PEMCuO-coated Ti sheets was determined in two experimental setups. In the first setup (unrinsed), the osteoblastic MG-63 cells were seeded directly onto the samples, while in the second setup (rinsed), the cells were seeded on the samples after they had been incubated for 24 h in media without cells.[66] The percentage of viable cells was determined by MTT assay.

A comparison of the rinsed and unrinsed test results revealed that the viability of MG-63 cells on rinsed surfaces was higher for all surfaces tested. In the case of PEM*n* and PEMCuO surfaces, the difference in cell viability determined by the two tests was significant (**Figure** 5a). The difference in the viability between the control cells and those grown on the investigated surfaces was significant in both tests. However, in all cases, the viability of MG-63 cells was above 70%. This is the threshold value for

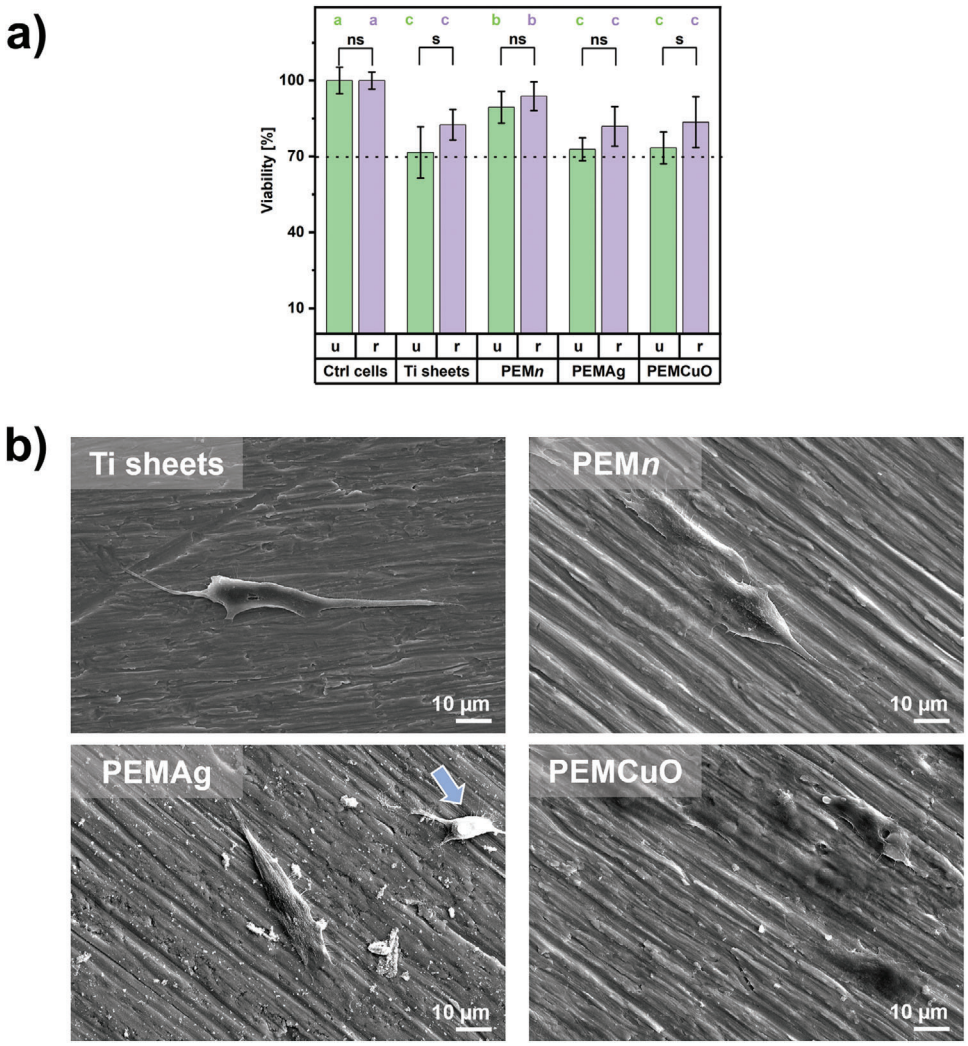

Figure 5. a) Cell viability of osteoblastic MG-63 cells on unrinsed and rinsed tested surfaces. Error bars represent standard deviation. b) SEM micrographs of MG-63 cells seeded after 24 h exposition to cell media. Ctrl cells – control cells, Ti sheets – original titanium surface, PEM*n* – Ti surface coated with PLL/PGA multilayer consisting of 10 bilayers without nanoparticles, PEMAg – Ti surface coated with PLL/PGA multilayer consisting of 10 bilayers with silver nanoparticles, PEMCuO – Ti surface coated with PLL/PGA multilayer consisting of 10 bilayers with copper oxide nanoparticles, u – unrinsed, r – rinsed. Means with different letters are significantly different. ns – not significant, s – significant difference, $p \leq 0.05$. The blue arrow denotes a cell with a round shape.

non-cytotoxic materials according to the criteria of the ISO 10993–5 protocol.

Cell viability was significantly higher on the PEM*n*-coated surfaces compared to the other surfaces tested under both conditions. This was not surprising as PLL/PGA PEMs have previously shown good biocompatibility.[67] PEMs ending with PGA have also shown good biocompatibility for osteoblast-like cells.[68] The addition of nanoparticles in PEM decreased cell viability, with no significant difference from the bare Ti surface, which had the lowest cell viability. A similar trend was observed with dopamine-modified alginate/chitosan PEM with or without embedded AgNPs.[39] Interestingly, no statistically significant difference in cell viability was observed for PEMAg and PEMCuO, despite a larger amount of CuONPs embedded within the PEM (Table 1). It should also be noted that the released compounds were also not cytotoxic (data not shown) despite the observed differences in the release of Ag and Cu ions (Table 1).

SEM images of the MG-63 cells confirm the lack of cytotoxic effect in all PEM samples (Figure 5b). Cells with a classical elongated shape with cytoplasmic extensions were observed on all coatings, further confirming their biocompatibility. However, in the case of PEMAg, round cells can be sparsely observed, implying some contact toxicity.

It is known that the cytotoxicity of AgNPs and CuONPs varies according to size, concentration, cell type, and ion release rate.[69] Surprisingly, as far as surface toxicity is concerned, there is scarce literature data on the cytotoxic effect of PEM with embedded AgNPs and CuONPs. Anandhakumar et al.[41] investigated the in situ preparation of AgNPs in (PAH)/dextran sulfate PEM and found that the prepared PEMs did not significantly affect the

growth of renal epithelial cells. Wang et al.[38] used a similar method to prepare chitosan/PVP films doped with AgNPs. They showed that the viability of human umbilical vein endothelial cells was significantly reduced when the concentration of $AgNO_3$ used for the in situ preparation of AgNPs was higher than 0.25 mM. Matijaković Mlinarić et al.[46] showed that the metabolic activity of immortalized human keratinocyte cells was not significantly reduced after the cells were exposed to cell media in which PAH/alginate multilayers with embedded CuONPs had been incubated for 24 h. However, the surface concentrations of Ag or Cu in PEMs were not reported in either study. To the best of our knowledge, Agarwal et al.[47] were the only ones to investigate the relationship between the amount of AgNPs loaded in PAH/poly(acrylic acid) (PAA) PEM and cytotoxicity. They found that PEMs containing ≈0.4 μg cm^{-2} Ag were not toxic to a murine fibroblast cell line NIH-3T3 but were effective against *S. epidermis*. Our results show that even a 5 times higher incorporated amount of Ag was not toxic to MG-63 cells. This could be a consequence of the different susceptibility of the different cell lines to Ag as well as the different polyelectrolytes used.

2.4. Antibacterial Activity

The formation of biofilms on implanted and indwelling medical devices represents a serious challenge in healthcare, as biofilms increase bacterial resistance to host immune response and antimicrobial agents, making infections difficult to treat.[70,71] Two bacterial strains were selected to evaluate the inhibition of surface biofilms: Gram-positive *S. aureus*, which is responsible for most IAIs,[53] and *P. aeruginosa*, the most common Gram-negative bacteria causing IAIs.[70]

The results of the biofilm assays are shown in **Figure 6**. In general, the surfaces tested inhibited *S. aureus* biofilm formation to a lesser extent than that of *P. aeruginosa*, which could potentially be due to the dense cell wall of Gram-positive bacteria being less permeable to metal ions.[72] Weak *S. aureus* biofilm was formed on bare Ti surfaces, while on PEM*n*-coated surfaces, moderate biofilm was formed. The surface properties of Ti surfaces, such as low surface roughness and hydrophobicity, probably contributed to lower bacterial adhesion.[73] In contrast, coating the Ti surface with PLL/PGA PEM altered the surface and made it conductive to bacteria, which is not surprising.[56] While PLL/PGA multilayer coatings improve cell compatibility, this benefit appears to come at the expense of increased bacterial adhesion. Nonetheless, the PEMCuO coating was the strongest biofilm inhibitor for both bacterial strains. It entirely inhibited the formation of *P. aeruginosa* biofilm, and only a weak biofilm of *S. aeruginosa* was formed. In addition, the statistically different OD values for *S. aureus* biofilm formation on PEM*n* and PEMCuO were obtained. The PEMAg coating was an efficient biofilm inhibitor only for *P. aeruginosa*.

PEMs embedded with Ag^+ ions are known for their antimicrobial efficacy, especially in combination with antiseptic agents, further driving research on PEMs containing AgNPs.[74,75] Interestingly, Dai et al. have shown that PEMs containing AgNPs have the same antibacterial effect as those containing Ag^+ ions. However, embedding nanoparticles in PEMs could be a preferable option to reduce Ag^+ bioaccumulation.[43]

Previous studies have shown that AgNPs are efficient in inhibiting the biofilm formation of both *S. aureus and P. aeruginosa*, with the extent of inhibition being dose-dependent and influenced by the type of stabilizing agent used for the AgNPs.[76–78] PAH/PAA PEM containing in situ synthesized AgNPs was found to be effective against both Gram-positive and Gram-negative bacteria.[79]

Moreover, Kruk et al.[45] showed that PEM with incorporated CuONPs exhibited antibacterial activity regardless of the number of PEM layers, suggesting a high contact mechanism of bacterial inhibition. CuONPs were also found to be effective against both bacteria, with higher efficacy observed in preventing the biofilm formation of *P. aeruginosa*.[80] PAH/alginate multilayers with embedded CuONPs were shown to be effective against *E. coli*, with alginate-terminating PEMs being more efficient.[46] To the best of our knowledge, there is no direct comparison of the efficacy of incorporated AgNPs or CuNPs/CuONPs against bacterial biofilm formation.

The SEM images of the PEMs with and without incorporated nanoparticles after the biofilm formation assay (Figure 6) revealed clusters of *S. aureus* cells and individual cells with a higher cell density on the PEM*n* surfaces, confirming the results of the biofilm formation assay. In the case of *P. aeruginosa*, scattered individual cells with coccoid morphology were observed, indicative of impaired growth. The relatively low cell densities correspond with the weak or no biofilm results obtained with the crystal violet assay.

Multilayers with incorporated metals and metal oxides are bactericidal LbL systems that can be based on either release, contact killing or a combination.[81] Since the multilayers investigated in this work released low amounts of Ag and Cu compared to the total amounts adsorbed (Table 1), it can be assumed that the mechanism of antibacterial activity of PEMAg and PEMCuO is mainly based on contact killing. This is in contrast to PEI/AgNPs PEM, where the release of Ag^+ ions was shown to be the dominant mechanism, although the contact mechanism could not be excluded.[44]

The mechanism of antibacterial action of AgNP and CuONP differs, although it is not fully understood for either nanoparticle.[25,82] In the case of AgNPs, in addition to the extracellular release of Ag^+ ions, release at the nanoparticle-cell interface also plays an important role in antibacterial activity. It has been shown that *P. aeruginosa* cells, which tend to attach to AgNPs, exhibited the highest sensitivity to different forms of AgNPs among the bacterial strains tested, including *S. aureus*.[83] Similarly, released copper atoms or copper ions (Cu^+ or Cu^{2+}) bind to negatively charged cell membranes, causing uneven distribution of negative charge across the membrane, leading to cell distortions, rupture, and leakage of cell contents, and copper can further interact with DNA and proteins, impairing normal cell functions leading to cell death.[19,84] In addition, CuONPs can eliminate bacteria by generating reactive oxygen species.[21,82]

Overall, antibacterial activity can be influenced by the size, shape, and charge of the nanoparticles, their aggregation state, and the ion release rate.[25,85]Although aggregated nanoparticles may limit interactions with the bacterial cell wall and consequently have a weaker effect on bacteria, PEMCuO was shown to still affect biofilm formation, but this may also be due to the

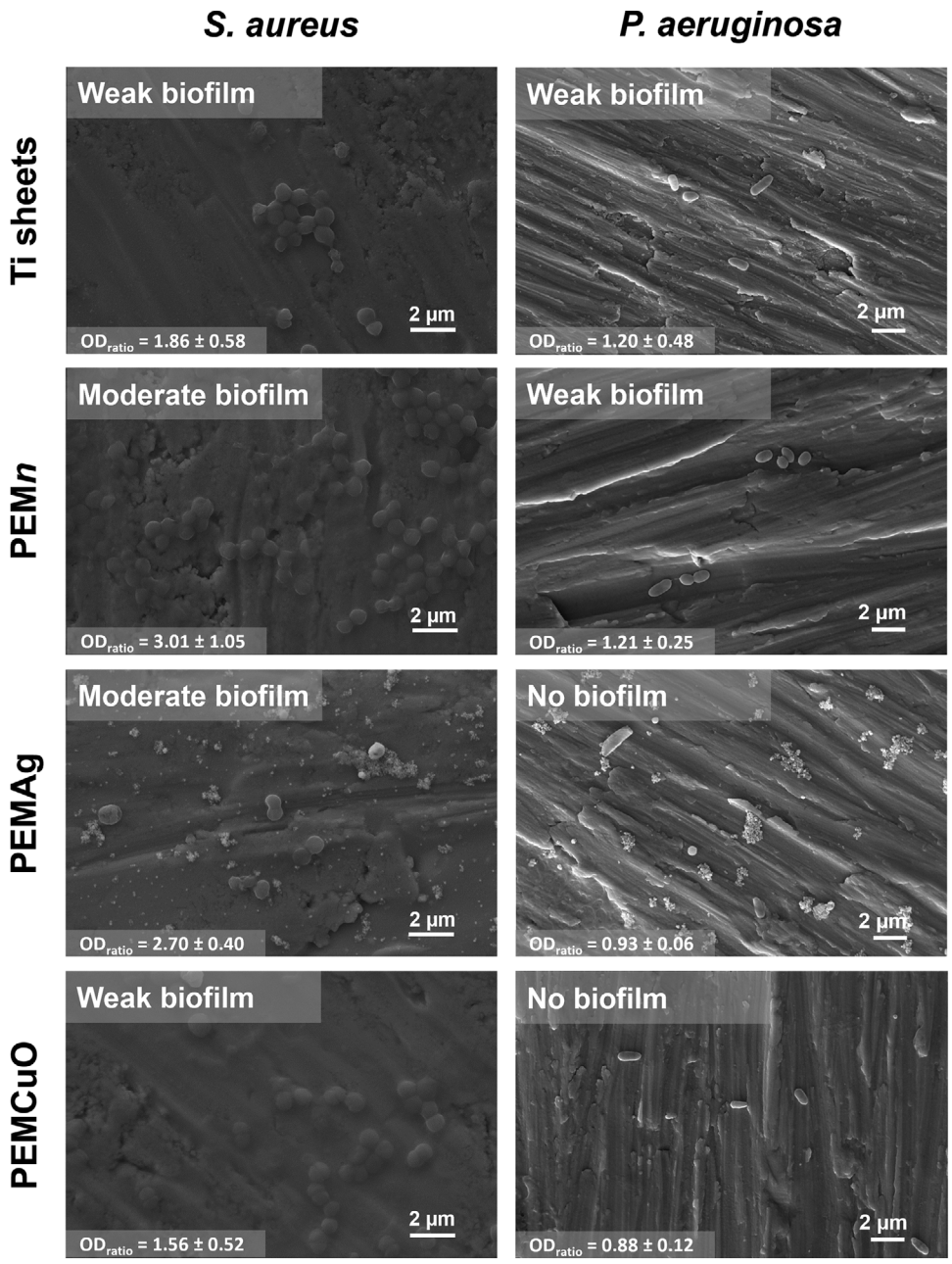

Figure 6. Representative SEM images of *Staphylococcus aureus* and *Pseudomonas aeruginosa* on Ti sheets – original titanium surface, PEM*n* – Ti surface coated with PLL/PGA multilayer consisting of 10 bilayers without nanoparticles, PEMAg – Ti surface coated with PLL/PGA multilayer consisting of 10 bilayers with silver nanoparticles, PEMCuO – Ti surface coated with PLL/PGA multilayer consisting of 10 bilayers with copper oxide nanoparticles. OD ratio ≤ 1 – no biofilm produced; 1 < OD ratio ≤ 2 – weak biofilm produced; 2 < OD ratio ≤ 4 – moderate biofilm produced; 4 < OD ratio – strong biofilm produced.

higher amount of adsorbed CuONPs. It is worth noting that Matijaković-Mlinarić et al.[46] have shown that in the case of CuONPs, morphology influence was less apparent compared to ZnO nanoparticles.

3. Conclusion

Antibacterial coatings for implanted medical devices attract attention as a potentially effective way to combat infections without promoting bacterial resistance. Given the varying surface composition, size, and topology of medical devices, it is essential to choose a versatile coating methodology and coating composition. The LbL build-up of PEMs offers this versatility and allows the incorporation of various antibacterial agents, such as AgNPs and CuONPs, both known for their broad-spectrum antibacterial activity.

In this study, we investigated and compared the physicochemical and biological properties of PEMs composed of

poly(amino acid) PLL and PGA, which serve as effective matrices. The successful embedding of AgNPs and CuONPs as anionic components in these PEMs resulted in coatings with distinct morphologies. It was revealed that a larger amount of CuONPs was adsorbed on the surface. In addition, the CuONPs were more aggregated on the surface, resulting in increased surface roughness and a lower contact angle of PEMCuO. Importantly, the PEMs were effective in preventing the burst release of total Ag and Cu, confirming the effectiveness of these coatings as sustained release systems.

Both PEMAg and PEMCuO were proven to be non-cytotoxic when tested with human osteoblastic MG-63 cells. This was probably due to the relatively low content of AgNPs and CuONPs entrapped on the surface and released into the medium, which did not significantly affect cell viability. More importantly, the presence of poly(amino acids) probably contributed substantially to the biocompatibility of the surfaces. In addition, both the PEMAg and PEMCuO coatings were effective in reducing biofilm formation by *S. aureus* and *P. aeruginosa*, with PEMCuO being a more efficient inhibitor for both bacteria.

The results obtained show that it is possible to achieve an antimicrobial effect with a minimal content of active agents, enabling retainment of biocompatibility. As the LbL method of preparation contributes to the scalability of the coating process, obtained results could have implications for the future design and application of PEM-based antimicrobial coatings. However, a limitation of this study is the difference in size, shape, and aggregation state of the nanoparticles used in this study, which limits a detailed direct comparison of the coatings studied. Further research should overcome these limitations by optimizing the size and distribution of the nanoparticles within the PEM layers. Furthermore, as the released particles and ions could have different effects on biological responses, further research should investigate this together with the long-term stability of metal release.

4. Experimental Section

Materials—Materials for AgNPs Synthesis and PEMs Build-Up: For the synthesis of AgNPs, silver nitrate ($AgNO_3$) was purchased from Alfa Aesar, while polyvinylpyrrolidone (PVP, $M_w = 40000$), ammonium (NH_3), D–(+)–glucose and sodium hydroxide (NaOH) were obtained from Sigma-Aldrich.

Poly-L-lysine hydrobromide (PLL, M_w = 30000-70000), poly-L-glutamic acid sodium salt (PGA, M_w = 50000-100000), 4-(2-hydroxyethyl)piperazine-1-ethanesulfonic acid (HEPES), sodium chloride (NaCl), copper oxide nanopowder (CuONPs) were purchased from Sigma-Aldrich. Sodium dodecyl sulfate (SDS), used for washing sensors, was also obtained from Sigma-Aldrich. Titanium sheets (99.6% purity, 0.5 mm x 10 mm x 10 mm) were purchased from HMW Hauner GmbH & Co. KG, Germany. They were cleaned by sonication in ethanol in three cycles, each lasting 10 min to ensure the removal of surface contaminants.

For ICP-MS analysis, nitric acid (HNO_3, 65%, Suprapur) was obtained from Merck, while the multielement reference standard and silver standard solution were obtained from Analytika and Fluka, respectively.

Materials for Cell Viability Assay and Cell Culturing: MG-63 cells (ECACC 86051601) were purchased from Sigma-Aldrich. Minimum Essential Medium Alpha 1 (α-MEM) and dimethyl sulfoxide (DMSO) were purchased from Corning, while Fetal Bovine Serum (FBS), amphotericin B, and gentamycin were obtained from PAN Biotech. Trypsin-EDTA, glutamine, and Dulbecco's Phosphate Buffered Saline (D-PBS), used to rinse the cell culture wells, were purchased from Dominique Dutscher. The MTT cell viability assay kit was purchased from Biotium.

Materials for Biofilm Formation Assay: Bacteria used for the biofilm formation assays included *S. aureus* DSM 1104 and *P. aeruginosa* DSM 22644. Tryptic soy agar and tryptic soy broth were obtained from Biolife, while D-(+)-glucose, phosphate buffer saline (PBS), and crystal violet 1% solution were obtained from Sigma-Aldrich. API Suspension Medium was purchased from bioMerieux, and formaldehyde 35% solution was from Kemika.

Synthesis of AgNPs: AgNPs were synthesized by the reduction of $AgNO_3$ with glucose, and stabilized with PVP, as described previously.[86] In short, $AgNO_3$ was added to the PVP solution under constant stirring to reach final concentrations of 1 mM $AgNO_3$ and 0.3% PVP. Then NH_3 (35%) was added, followed by the gradual addition of glucose solution at a rate of approximately one drop per second. Finally, NaOH was added, and the resulting reaction mixture was kept at 40 °C for another 30 min with continued stirring for another 20–30 min. The resulting suspension was centrifuged twice at 3500 x g for 15 min. The supernatant was discarded, and the precipitate was resuspended in ultrapure water. The concentration of AgNPs was determined by inductively coupled plasma mass spectrometry. The suspension was stored at 4 °C in the dark until further use.

Methods—PEM Build-Up: The solutions (γ = 1 mg mL^{-1}) of the PLL and PGA were freshly prepared for each experiment by dissolving the chemicals in HEPES/NaCl buffer. PEMs were prepared by alternately immersing substrates into PLL and PGA solutions, each adsorption step lasting 15 min. Loosely bound PEs were removed by rinsing three times with HEPES/NaCl for 5 min. The deposition started with PLL and continued until the desired number of bilayers was reached, up to a total number of 10 bilayers, forming the $(PLL/PGA)_{10}$ multilayer (PEM*n*).

For the preparation of multilayers with embedded nanoparticles, nanoparticle suspensions of AgNPs or CuONPs (50 mg L^{-1}, HEPES/NaCl) were used as the anionic component instead of PGA in the deposition of the 3rd and 8th bilayers. This resulted in the formation of $(PLL/PGA)_2(PLL/AgNPs)(PLL/PGA)_4(PLL/AgNPs)(PLL/PGA)_2$ (PEMAg) or $(PLL/PGA)_2(PLL/CuONPs)(PLL/PGA)_4(PLL/CuONPs)(PLL/PGA)_2$ (PEMCuO).

Prepared PEMs were stored at 4 °C until further use.

Quartz-Crystal Microbalance with Dissipation Monitoring (QCM-D): The PEM build-up was monitored in situ using the Q-Sense E1 instrument (Biolin Scientific, Sweden). Titanium sensors (QSX 310 Ti, Biolin Scientific, Sweden) with a fundamental resonance frequency of 5 MHz were used. Before each PEM build-up, sensors were cleaned by immersion in 2% SDS for 30 min, then rinsed with ultrapure water and dried with nitrogen gas. The dried sensors were treated with O_2 plasma in the Diener Zepto plasma oven for 10 min.

At the beginning of the PEM deposition measurement, the ultrapure water was pumped through the QCM-D flow cell. To determine the baseline values of Δf and ΔD, HEPES/NaCl buffer solution was pumped through the cell before the first deposition step. PLL and PGA polyelectrolyte solutions were then sequentially added, each pumped for 10 min, with a 5 min buffer flow after each polyelectrolyte adsorption step. This cycle was repeated until 10 bilayers were formed. AgNPs or CuONPs suspensions (γ = 50 mg L^{-1}) were added in place of the polyanionic PGA solution during the 3rd and 8th bilayer build-up. The flow was maintained at 150 µL min^{-1} using a peristaltic pump (Ismatec^{TM} Reglo Digital Pump, IDEX Health & Science, Germany) and the temperature was kept constant at 23.00 ± 0.02 °C throughout the measurement. The parameter changes were recorded for several odd harmonics, however values of the 3rd harmonic parameters were used for the graphical analysis.

The Voigt model was used to calculate the thickness since significant changes in dissipation were observed ($\Delta D > 0$) which limits the use of the Sauerbrey equation.[60] The changes in frequency (Δf) and (ΔD) were described by the following Equations (1) and (2):[87]

$$\Delta f \approx -\frac{1}{2\pi\rho_0 d_0}\left\{\frac{\eta_2}{\delta_2} + d_1\rho_1\omega_1 - 2d_1\left(\frac{\eta_2}{\delta_2}\right)^2\frac{\eta_1\omega^2}{\mu_1^2+\omega^2\eta_1^2}\right\} \quad (1)$$

$$\Delta D \approx \frac{1}{2\pi f \rho_0 d_0}\left\{\frac{\eta_2}{\delta_2} + 2d_1\left(\frac{\eta_2}{\delta_2}\right)^2 \frac{\mu_1\omega^2}{\mu_1^2+\omega^2\eta_1^2}\right\} \quad (2)$$

In Equations (1) and (2), f stands for the resonant frequency, ρ for the density, d for the thickness, η for the viscosity, μ for the modulus of elasticity, and ω for the angular frequency ($\omega = 2\pi f$), and $\delta = \sqrt{\frac{2\eta}{\rho\omega}}$. The index 0 stands for the quartz crystal, 1 for the adsorbed layers, and 2 for the liquid medium. The fitting was performed with the software QTools 3 (Biolin Scientific, Sweden). Overtones of frequency considered were 3rd, 5th, 7th, 9th, and 11th.

Dynamic and Electrophoretic Light Scattering (DLS and ELS): The size distribution and zeta potential of AgNPs and CuONPs suspended in HEPES/NaCl buffer were determined by DLS and ELS using a photon correlation spectrophotometer, Zetasizer Nano ZS (Malvern Instruments, Worcestershire, United Kingdom) with a 532 nm "green" laser. For DLS measurements, the intensity of the scattered light was monitored at the angle of 173 °. To avoid possible overestimation of particle size due to the scattering of larger particles, the hydrodynamic diameter (d_h) was obtained as a value at the peak maximum of the size volume distribution function. The zeta potential (ζ) of the nanoparticles was calculated from the electrophoretic mobility measurements using the Henry equation with the Smoluchowski approximation. Each sample was measured five times, and representative data are shown. Data processing was carried out using Zetasizer software 7.13 (Malvern Instrument Worcestershire, United Kingdom). All measurements were performed at 25.0 ± 0.1 °C.

Transmission Electron Microscopy (TEM): TEM images of AgNPs were obtained using LaB Philips CM200 TEM and Jeol Jem 1010 operated at 80 kV. For TEM/SAED analysis, a drop of the nanoparticle suspension was placed on a copper grid covered with a hollow Formvar membrane. The excess solution was adsorbed with filter paper, and the precipitate was washed three times with a drop of ultrapure water. After removing excess water, the samples were dried under a stream of nitrogen. The samples were stored in a desiccator until further analysis.

Scanning Electron Microscopy (SEM): Scanning electron micrographs of the CuONPs were obtained with a Zeiss Crossbeam 550 SEM (Germany) at voltages between 5 and 10 kV. The elemental composition of the PEM samples was analyzed using the Oxford Ultim Max 170 EDS detector (United Kingdom) integrated into the Zeiss Crossbeam 550 SEM setup. The EDS measurements were performed at an accelerating voltage of 20 kV.

For visualization of MG-63 and bacterial cells by SEM, samples were washed with PBS, fixed with 4% glutaraldehyde, and dried with a series of graded ethanol concentrations. These included a sequence of 10-min immersions in 70, 80, and 90% ethanol, followed by a final overnight immersion in 100% ethanol. Once dehydrated, the samples were sputter-coated with gold for SEM imaging[88] Hitachi SU5000 with EDS/WDS (Thermo Scientific) was used for imaging MG-63 cells. Imaging of bacterial cells was conducted with the Zeiss Crossbeam 550 SEM (Germany) and the Axia ChemiSEM (Thermo Fisher Scientific, USA).

Particle Size Measurements: The particle size distributions of AgNPs and CuONPs from SEM and TEM micrographs were determined using the image analysis software Image J 1.48v (freely available at https://imagej.net/ij/). The results were expressed as the mean ± standard deviation of 50 measured particles.

Atomic Force Microscopy (AFM): The samples for AFM were prepared on mica substrates and air-dried before analysis. Topography and roughness measurements were performed using a Park NX20 AFM (Park Systems, South Korea) in non-contact mode. These measurements were performed under ambient air conditions using a PPP-NCHR XY tip with a 30 nm thick aluminum coating on the detector side (nominal mean width 30 µm, nominal thickness 4 µm, nominal length 125 µm, nominal force constant 42 N m^{-1}, nominal resonance frequency 330 kHz). The linear scanning rate was 0.15 Hz with the set point 9–11 nm. The image size was set to 5 µm × 5 µm with a resolution of 512 pixels × 512 pixels. The open-source software Gwyddion 2.61 was used for data processing and analysis.

Inductively Coupled Plasma Mass Spectrometry (ICP-MS): To determine the Ag concentration in the synthesized AgNPs suspension and the total amount of Ag and Cu incorporated in PEMs, the samples were dissolved in 5 mL of 2% (v/v) HNO_3. For the analysis, these solutions were treated without further dilution, and In (1 µg L^{-1}) was added as an internal standard. The release of Ag and Cu from PEMs was investigated by immersing the samples in PBS for 1, 4, and 24 h, after which an aliquot of the solution was withdrawn for analysis. These aliquots were then diluted 100-fold and acidified with 2% (v/v) HNO_3 to prepare them for measurement. In this way, potentially present nanoparticles were dissolved, and total concentrations of Ag and Cu in the samples were determined by ICP-MS using the 8900 ICP-QQQ (Agilent, USA) and expressed as cumulative ionic species released per surface area (µg cm^{-2}). The element concentrations were determined by external calibration with standard solutions. Standards were prepared by appropriate dilution of a multi-element reference standard (100 ± 0.2 mg L^{-1}) containing Cu and a single standard solution of Ag (1.000 ± 0.002 g L^{-1}). The quality control of the measurements was performed by simultaneously measuring the blank samples and the internal control samples.

Wettability: The wetting properties of bare and PEM-coated Ti sheets were assessed by static contact angle measurements with the DSA25E instrument (Krüss, Germany) at room temperature and ambient atmospheric conditions. Still images of a drop of 1 µl ultrapure water deposited on the surface were recorded and fitted with Krüss Advance software. At least 10 measurements were performed for each sample.

Cell Viability Assays: The human osteoblastic MG-63 cells were cultured in 25 or 75 cm^2 flasks (Thermo Fisher Scientific, USA) in complete media consisting of Minimum Essential Medium Alpha 1 supplemented with 10% fetal bovine serum, 50 µg mL^{-1} gentamicin, 0.25 µg mL^{-1} amphotericin B and 2 mmol L^{-1} glutamine. Subculture of cells was performed at 70% confluence (every 3–4 days) by detaching the cells with trypsin 0.05% and diluting the detached cells in new complete media. Cells were incubated under standard conditions (37 °C, 5% CO_2, humidified atmosphere).

The samples, bare Ti sheets, PEM*n*, PEMAg, and PEMCuO, were sterilized by UV irradiation for 15 min on each side. The experimental design for assay included two different experimental setups to assess cytotoxicity: a) cytotoxicity of the samples that came into direct contact with the cells (unrinsed), and b) cytotoxicity of the samples that were rinsed with the media for 24 h before the cells were added (rinsed).[66]

Cells were seeded onto the sample surfaces in the two aforementioned experimental setups at a density of $1{\cdot}10^5$ cells cm^{-2} in 24-wells microplates (3524, Corning, USA) and cultured in complete cell media, using media with and without cells as positive and negative controls, respectively. After 24 h of growth, a fresh complete cell medium with MTT was added to each well according to the manufacturer's instructions (Biotium, USA). After 3 h of incubation to allow the formation of formazan crystals, DMSO was added to dissolve the crystals by gentle mixing. Aliquots of 100 µL of each supernatant were transferred to a 96-wells microplate (3596, Corning, USA), and the absorbance was measured at 570 nm and 630 nm using the Infinite M200 PRO microplate reader (TECAN, Switzerland). The percentage of viable cells for each sample was calculated according to the following Equation (3):

$$\%\ viability = \frac{OD_{test} - OD_{blank}}{OD_{control} - OD_{blank}} \times 100 \quad (3)$$

where OD is optical density, which is the result of $A_{570} - A_{630}$ for each condition. OD_{blank} refers to the optical density of the negative control, and $OD_{control}$ refers to the optical density of the positive control. The data corresponds to four different replicates for each condition.

Bacterial Adhesion and Biofilm Formation Assay: Bare Ti sheets, PEM*n*, PEMAg, and PEMCuO samples were prepared for bacterial adhesion and biofilm formation assays with Gram-positive *S. aureus* and Gram-negative *P. aeruginosa* bacterial strains. Prior to testing, samples were sterilized under UV light for 30 min. Eight replicates were prepared: three for each bacterial strain and two for negative controls.

Bacterial inoculum was prepared from fresh overnight cultures on tryptic soy agar, which turbidity was adjusted to 0.5 MacFarland with sterile 5 mL 0.85% API Suspension Medium and then diluted to a final concentration of $5{\cdot}10^4$ CFU mL^{-1} in tryptic soy broth supplemented with 1% glucose. This was used for the overnight incubation of the samples in 24-wells microplates at 35 °C in an aerobic atmosphere to facilitate bacterial growth and biofilm formation. After overnight incubation, the samples were removed from wells and washed three times in PBS to remove loosely attached bacteria and fixed with formaldehyde for 15 min. Subsequently, the samples were washed again and stained with 0.1% crystal violet for 15 min. The stained samples were then rinsed, dried at 60 °C for 45 min, and treated with 96% ethanol for 30 min to resolubilize the bound crystal violet. A 100 µL aliquot of the resulting solution was transferred to a 96-well plate, and absorbance was measured at a wavelength of 590 nm (OD590) using an Infinite 200 PRO microplate reader (TECAN, Grödig, Austria). The average absorbance values and standard deviation were calculated. The OD cut-off value used for biofilm quantification was determined by adding three times the standard deviation to the average value of the blanks (samples without bacteria). The quantity of attached bacteria, indicating biofilm formation, was obtained by dividing the average absorbance values of the bacterial samples by the OD cut-off value. Accordingly, biofilm formation was categorized as follows: an OD ratio of 0–1 indicated samples with no biofilm formation, 1–2 indicated weak biofilm formation, 2–4 indicated moderate biofilm formation and values above 4 indicated strong biofilm formation.[89,90]

Statistical Analysis: All data throughout the manuscript are presented as mean ± standard deviation, if not specified otherwise. Statistical analyses were done in Origin Pro 9.0 software. The choice of statistical test was based on the results of the Shapiro-Wilk normality test. For normally distributed data, a one-way ANOVA followed by a Tukey post-hoc test was used. For non-normally distributed data, the Kruskal-Wallis ANOVA and Dunn's post-hoc test were performed. In all analyses, statistical significance was determined with a threshold of $\alpha = 0.05$.

Supporting Information

Supporting Information is available from the Wiley Online Library or from the author.

Acknowledgements

This work has received funding from the European Union's Horizon 2020 research and innovation program under the Marie Skłodowska-Curie Actions (H2020-MSCA-ITN) as part of the project AIMed-Antimicrobial Integrated Methodologies for Orthopedic applications (grant agreement no. 861138).

Conflict of Interest

The authors declare no conflict of interest.

Data Availability Statement

The data that support the findings of this study are available from the corresponding author upon reasonable request.

Keywords

antibacterial coatings, copper oxide nanoparticles, cytotoxicity, polyelectrolyte multilayers, silver nanoparticles

Received: July 29, 2024
Revised: November 22, 2024
Published online: December 4, 2024

[1] K. Ivanova, A. Bassegoda, T. Tzanov, *Handb. Antimicrob. Coat.* **2018**, 487.
[2] M. Navarro, A. Michiardi, O. Castaño, J. A. Planell, *J. R. Soc. Interface* **2008**, *5*, 1137.
[3] A. Bussooa, S. Neale, J. R. Mercer, *Sensors* **2018**, *18*, 2018.
[4] J. W. Costerton, P. S. Stewart, E. P. Greenberg, *Science* **1999**, *284*, 1318.
[5] D. G. Kennedy, A. M. O'Mahony, E. P. Culligan, C. M. O'Driscoll, K. B. Ryan, *Antibiotics* **2022**, *11*, 1822.
[6] Z. Wu, B. Chan, J. Low, J. J. H. Chu, H. W. D. Hey, A. Tay, *Bioact. Mater.* **2022**, *16*, 249.
[7] C. Llor, L. Bjerrum, *Ther. Adv. Drug Saf.* **2014**, *5*, 229.
[8] F. Prestinaci, P. Pezzotti, A. Pantosti, *Pathog. Glob. Health* **2015**, *109*, 309.
[9] C. L. Romanò, H. Tsuchiya, I. Morelli, A. G. Battaglia, L. Drago, *Bone J. Res.* **2019**, *8*, 199.
[10] T. F. Moriarty, R. Kuehl, T. Coenye, W.-J. Metsemakers, M. Morgenstern, E. M. Schwarz, M. Riool, S. A. J. Zaat, N. Khana, S. L. Kates, R. G. Richards, *EFORT Open Rev.* **2016**, *1*, 89.
[11] V. Allizond, S. Comini, A. M. Cuffini, G. Banche, *Antibiotics* **2022**, *11*, 529.
[12] L. Wang, C. Hu, L. Shao, *Int. J. Nanomed.* **2017**, *12*, 1227.
[13] J. L. Falconer, D. W. Grainger, in *1.4 Silver Antimicrobial Biomaterials, in Compr. Biomater. II*, Elsevier, Amsterdam, Netherlands, **2017**, *1*, pp. 79–91.
[14] M. Ip, S. L. Lui, V. K. M. Poon, I. Lung, A. Burd, *J. Med. Microbiol.* **2006**, *55*, 59.
[15] M. Rai, A. Yadav, A. Gade, *Biotechnol. Adv.* **2009**, *27*, 76.
[16] S. Kittler, C. Greulich, J. Diendorf, M. Köller, M. Epple, *Chem. Mater.* **2010**, *22*, 4548.
[17] S. L. Percival, P. G. Bowler, D. Russell, *J. Hosp. Infect.* **2005**, *60*, 1.
[18] R. Norton, P. J. Finley, *J. Wound Care* **2021**, *30*, 238.
[19] N. Bharadishettar, U. Bhat K, D. Bhat Panemangalore, *Metals* **2021**, *11*, 711.
[20] (Ed.: E. J. Massaro), *Handbook of Copper Pharmacology and Toxicology*, Humana Press, Totowa, NJ, **2002**.
[21] X. Li, Y. Cong, M. Ovais, M. B. Cardoso, S. Hameed, R. Chen, M. Chen, L. Wang, *Nanomed. Nanobiotechnol.* **2023**, *15*, e1888.
[22] Y. Liu, J. Zhu, L. Xu, B. Wang, W. Lin, Y. Luo, *Front. Mol. Biosci.* **2022**, *9*, 1065265.
[23] J. R. Turnlund, W. R. Keyes, S. K. Kim, J. M. Domek, *Am. J. Clin. Nutr.* **2005**, *81*, 822.
[24] J. J. Hostynek, H. I. Maibach, *Dermatol. Ther.* **2004**, *17*, 328.
[25] Y. N. Slavin, J. Asnis, U. O. Häfeli, H. Bach, *J. Nanobiotechnol.* **2017**, *15*, 65.
[26] L. A. Tamayo, P. A. Zapata, N. D. Vejar, M. I. Azócar, M. A. Gulppi, X. Zhou, G. E. Thompson, F. M. Rabagliati, M. A. Páez, *Mater. Sci. Eng. C* **2014**, *40*, 24.
[27] S. Ferraris, S. Spriano, *Mater. Sci. Eng. C* **2016**, *61*, 965.
[28] P. Makvandi, C. Wang, E. N. Zare, A. Borzacchiello, L. Niu, F. R. Tay, *Adv. Funct. Mater.* **2020**, *30*, 1910021.
[29] L. Séon, P. Lavalle, P. Schaaf, F. Boulmedais, *Langmuir* **2015**, *31*, 12856.
[30] G. Decher, J. D. Hong, J. Schmitt, *Thin Solid Films* **1992**, *210–211*, 831.
[31] J. M. Silva, R. L. Reis, J. F. Mano, *Small* **2016**, *12*, 4308.
[32] S. Srivastava, N. A. Kotov, *Acc. Chem. Res.* **2008**, *41*, 1831.
[33] E. V. Lengert, S. I. Koltsov, J. Li, A. V. Ermakov, B. V. Parakhonskiy, E. V. Skorb, A. G. Skirtach, *Coatings* **2020**, *10*, 1131.
[34] K. Ariga, J. P. Hill, Q. Ji, *Phys. Chem. Chem. Phys.* **2007**, *9*, 2319.
[35] M. Criado-Gonzalez, C. Mijangos, R. Hernández, *Polymers* **2021**, *13*, 2254.
[36] T. He, V. Chan, *J. Biomed. Mater. Res., Part A* **2010**, *95A*, 454.
[37] X. Huang, M. J. Bolen, N. S. Zacharia, *Phys. Chem. Chem. Phys.* **2014**, *16*, 10267.

[38] B.-L. Wang, X.-S. Liu, Y. Ji, K.-F. Ren, J. Ji, *Carbohydr. Polym.* **2012**, *90*, 8.
[39] X. Zhang, Z. Li, X. Yuan, Z. Cui, H. Bao, X. Li, Y. Liu, X. Yang, *Mater. Sci. Eng. C* **2013**, *33*, 2816.
[40] W. Zhang, A. Zhang, Y. Guan, Y. Zhang, X. X. Zhu, *J. Mater. Chem.* **2011**, *21*, 548.
[41] S. Anandhakumar, A. M. Raichur, *Acta Biomater.* **2013**, *9*, 8864.
[42] J. Wei, L. Wang, X. Zhang, X. Ma, H. Wang, Z. Su, *Langmuir* **2013**, *29*, 11413.
[43] J. Dai, M. L. Bruening, *Nano Lett.* **2002**, *2*, 497.
[44] T. Kruk, K. Szczepanowicz, D. Kręgiel, L. Szyk-Warszyńska, P. Warszyński, *Colloids Surf. B Biointerfaces* **2016**, *137*, 158.
[45] T. Kruk, M. Gołda-Cępa, K. Szczepanowicz, L. Szyk-Warszyńska, M. Brzychczy-Włoch, A. Kotarba, P. Warszyński, *Colloids Surf. B Biointerfaces* **2019**, *181*, 112.
[46] N. M. Mlinarić, S. Altenried, A. Selmani, J. Nikolić, A. Učakar, A. Zore, A. Abram, S. Lehner, A. S. Škapin, M. Kušter, E. Roblegg, D. Kovačević, Q. Ren, K. Bohinc, *ACS Appl. Nano Mater.* **2024**, *7*, 12550.
[47] A. Agarwal, T. L. Weis, M. J. Schurr, N. G. Faith, C. J. Czuprynski, J. F. McAnulty, C. J. Murphy, N. L. Abbott, *Biomaterials* **2010**, *31*, 680.
[48] M. Mesić, T. Klačić, A. Abram, K. Bohinc, D. Kovačević, *Polymers* **2022**, *14*, 2566.
[49] K. Numata, *Polym. J.* **2015**, *47*, 537.
[50] R. Schade, M. D. Sikirić, S. Lamolle, H. J. Ronold, S. P. Lyngstadass, K. Liefeith, F. Cuisinier, H. Füredi-Milhofer, *J. Biomed. Mater. Res., Part A* **2010**, *95A*, 691.
[51] D. Kovačević, R. Pratnekar, K. Godič Torkar, J. Salopek, G. Dražić, A. Abram, K. Bohinc, *Polymers* **2016**, *8*, 345.
[52] M. Geetha, A. K. Singh, R. Asokamani, A. K. Gogia, *Prog. Mater. Sci.* **2009**, *54*, 397.
[53] G. Pietrocola, D. Campoccia, C. Motta, L. Montanaro, C. R. Arciola, P. Speziale, *Int. J. Mol. Sci.* **2022**, *23*, 5958.
[54] M. Elimelech, *Particle deposition and aggregation: measurement, modelling, and simulation*, Butterworth-Heinemann, Woburn, **1998**.
[55] N. Akaighe, S. W. Depner, S. Banerjee, V. K. Sharma, M. Sohn, *Sci. Total Environ.* **2012**, *441*, 277.
[56] F. Boulmedais, B. Frisch, O. Etienne, P. Lavalle, C. Picart, J. Ogier, J.-C. Voegel, P. Schaaf, C. Egles, *Biomaterials* **2004**, *25*, 2003.
[57] P. H. Lavalle, C. Gergely, F. J. G. Cuisinier, G. Decher, P. Schaaf, J. C. Voegel, C. Picart, *Macromolecules* **2002**, *35*, 4458.
[58] L. Richert, Y. Arntz, P. Schaaf, J.-C. Voegel, C. Picart, *Surf. Sci.* **2004**, *570*, 13.
[59] P. Lavalle, V. Vivet, N. Jessel, G. Decher, J.-C. Voegel, P. J. Mesini, P. Schaaf, *Macromolecules* **2004**, *37*, 1159.
[60] A. D. Easley, T. Ma, C. I. Eneh, J. Yun, R. M. Thakur, J. L. Lutkenhaus, *J. Polym. Sci.* **2022**, *60*, 1090.
[61] S. T. Dubas, J. B. Schlenoff, *Macromolecules* **1999**, *32*, 8153.
[62] T. J. Halthur, U. M. Elofsson, *Langmuir* **2004**, *20*, 1739.
[63] A. Bratek-Skicki, M. Sadowska, J. Maciejewska-Prończuk, Z. Adamczyk, *Nanomaterials* **2021**, *11*, 145.
[64] G. Bogdanovic, T. Sennerfors, B. Zhmud, F. Tiberg, *J. Colloid Interface Sci.* **2002**, *255*, 44.
[65] B. Zhang, K. Rane, M. Piri, L. Goual, *Pet. Sci.* **2023**, *20*, 2852.
[66] V. Stranak, H. Wulff, H. Rebl, C. Zietz, K. Arndt, R. Bogdanowicz, B. Nebe, R. Bader, A. Podbielski, Z. Hubicka, R. Hippler, *Mater. Sci. Eng. C* **2011**, *31*, 1512.
[67] D. Zhou, H. Xiao, F. Meng, S. Zhou, J. Guo, X. Li, X. Jing, Y. Huang, *Bioconjug. Chem.* **2012**, *23*, 2335.
[68] P. Tryoen-Tóth, D. Vautier, Y. Haikel, J.-C. Voegel, P. Schaaf, J. Chluba, J. Ogier, *J. Biomed. Mater. Res.* **2002**, *60*, 657.
[69] F. Amaro, Á. Morón, S. Díaz, A. Martín-González, J. C. Gutiérrez, *Microorganisms* **2021**, *9*, 364.
[70] C. R. Arciola, D. Campoccia, L. Montanaro, *Nat. Rev. Microbiol.* **2018**, *16*, 397.
[71] Y. Zheng, L. He, T. K. Asiamah, M. Otto, *Environ. Microbiol.* **2018**, *20*, 3141.
[72] E. M. Hia, S. R. Jang, B. Maharjan, J. Park, C. H. Park, *Colloids Surf. B Biointerfaces* **2024**, *236*, 113804.
[73] L. K. Zaugg, M. Astasov-Frauenhoffer, O. Braissant, I. Hauser-Gerspach, T. Waltimo, N. U. Zitzmann, *Clin. Oral Implants Res.* **2017**, *28*, 469.
[74] J. C. Grunlan, J. K. Choi, A. Lin, *Biomacromolecules* **2005**, *6*, 1149.
[75] Z. Shi, K. G. Neoh, S. P. Zhong, L. Y. L. Yung, E. t. Kang, W. Wang, *J. Biomed. Mater. Res., Part A* **2006**, *76A*, 826.
[76] R. Mann, A. Holmes, O. McNeilly, R. Cavaliere, G. A. Sotiriou, S. A. Rice, C. Gunawan, *J. Nanobiotechnology* **2021**, *19*, 291.
[77] B. Hosnedlova, D. Kabanov, M. Kepinska, V. H. B. Narayanan, A. A. Parikesit, C. Fernandez, G. Bjørklund, H. V. Nguyen, A. Farid, J. Sochor, A. Pholosi, M. Baron, M. Jakubek, R. Kizek, *Nanomaterials* **2022**, *12*, 2183.
[78] N. Palanisamy, N. Ferina, A. Amirulhusni, Z. Mohd-Zain, J. Hussaini, L. Ping, R. Durairaj, *J. Nanobiotechnology* **2014**, *12*, 2.
[79] D. Lee, R. E. Cohen, M. F. Rubner, *Langmuir* **2005**, *21*, 9651.
[80] L. R. Christena, V. Mangalagowri, P. Pradheeba, K. B. A. Ahmed, B. I. S. Shalini, M. Vidyalakshmi, V. Anbazhagan, N. S. Subramanian, *RSC Adv.* **2015**, *5*, 12899.
[81] X. Zhu, X. J. Loh, *Biomater. Sci.* **2015**, *3*, 1505.
[82] G. Vasiliev, A.-L. Kubo, H. Vija, A. Kahru, D. Bondar, Y. Karpichev, O. Bondarenko, *Sci. Rep.* **2023**, *13*, 9202.
[83] O. Bondarenko, A. Ivask, A. Käkinen, I. Kurvet, A. Kahru, *PLoS One* **2013**, *8*, e64060.
[84] J. Yu, X. Huang, F. Ren, H. Cao, M. Yuan, T. Ye, F. Xu, *Appl. Organomet. Chem.* **2024**, *38*, e7506.
[85] A. Ivanova, K. Ivanova, J. Hoyo, T. Heinze, S. Sanchez-Gomez, T. Tzanov, *ACS Appl. Mater. Interfaces* **2018**, *10*, 3314.
[86] I. Vinković Vrček, I. Pavičić, T. Crnković, D. Jurašin, M. Babič, D. Horák, M. Lovrić, L. Ferhatović, M. Ćurlin, S. Gajović, *RSC Adv.* **2015**, *5*, 70787.
[87] N. Parveen, P. K. Jana, M. Schönhoff, *Polymers* **2019**, *11*, 1285.
[88] R. Ali, K. El-Boubbou, M. Boudjelal, *MethodsX* **2021**, *8*, 101521.
[89] S. Stepanović, D. Vuković, V. Hola, G. D. Bonaventura, S. Djukić, I. Ćirković, F. Ruzicka, *APMIS* **2007**, *115*, 891.
[90] S. Barkarmo, D. Longhorn, K. Leer, C. B. Johansson, V. Stenport, S. Franco-Tabares, S. A. Kuehne, R. Sammons, *Clin. Exp. Dent. Res.* **2019**, *5*, 427.